Large-scale instability in a sheared nonhelical turbulence: Formation of vortical structures

Tov Elperin,[*] Ilia Golubev,[†] Nathan Kleeorin,[‡] and Igor Rogachevskii[§]

The Pearlstone Center for Aeronautical Engineering Studies, Department of Mechanical Engineering,
Ben-Gurion University of the Negev, Beer-Sheva 84105, P. O. Box 653, Israel
(Received 11 July 2007; published 14 December 2007)

We study a large-scale instability in a sheared nonhelical turbulence that causes generation of large-scale vorticity. Three types of the background large-scale flows are considered, i.e., the Couette and Poiseuille flows in a small-scale homogeneous turbulence, and the "log-linear" velocity shear in an inhomogeneous turbulence. It is known that laminar plane Couette flow and antisymmetric mode of laminar plane Poiseuille flow are stable with respect to small perturbations for any Reynolds numbers. We demonstrate that in a small-scale turbulence under certain conditions the large-scale Couette and Poiseuille flows are unstable due to the large-scale instability. This instability causes formation of large-scale vortical structures stretched along the mean sheared velocity. The growth rate of the large-scale instability for the "log-linear" velocity shear is much larger than that for the Couette and Poiseuille background flows. We have found a turbulent analogue of the Tollmien-Schlichting waves in a small-scale sheared turbulence. A mechanism of excitation of turbulent Tollmien-Schlichting waves is associated with a combined effect of the turbulent Reynolds stress-induced generation of perturbations of the mean vorticity and the background sheared motions. These waves can be excited even in a plane Couette flow imposed on a small-scale turbulence when perturbations of mean velocity depend on three spatial coordinates. The energy of these waves is supplied by the small-scale sheared turbulence.

PACS number(s): 47.27.N−, 47.27.nd

I. INTRODUCTION

Large-scale vortical structures are universal features observed in geophysical, astrophysical, and laboratory flows (see, e.g., [1–6]). Formation of vortical structures is related to the Prandtl secondary flows (see, e.g., [7–10]). A lateral stretching (or "skewing") by an existing shear generates streamwise vorticity that results in formation of the first kind of the Prandtl secondary flows. In turbulent flow the large-scale vorticity is generated by the divergence of the Reynolds stresses. This mechanism determines the second kind of the Prandtl turbulent secondary flows [10].

The generation of large-scale vorticity in a homogeneous nonhelical turbulence with an imposed large-scale linear velocity shear has been recently studied in [11]. Let us discuss a mechanism of this phenomenon. The equation for the mean vorticity $\mathbf{W} = \boldsymbol{\nabla} \times \mathbf{U}$ read

$$\frac{\partial \mathbf{W}}{\partial t} = \boldsymbol{\nabla} \times (\mathbf{U} \times \mathbf{W} + \mathbf{F} - \nu \boldsymbol{\nabla} \times \mathbf{W}), \tag{1}$$

where $\mathbf{U}$ is the mean fluid velocity, $\mathbf{F}_i = -\nabla_j \langle u_i u_j \rangle$ is the effective force caused by velocity fluctuations, $\mathbf{u}$, and ν is the kinematic viscosity. The first term, $\mathbf{U} \times \mathbf{W}$, in Eq. (1) determines laminar effects of the mean vorticity production caused by the sheared motions, while the effective force $\mathbf{F}$ determines the turbulent effects on the mean fluid flow. Let us consider a simple large-scale linear velocity shear $\mathbf{U}^{(s)} = (0, Sx, 0)$ imposed on the small-scale nonhelical turbulence.

*elperin@bgu.ac.il; URL: http://www.bgu.ac.il/~elperin
†golubev@bgu.ac.il
‡nat@menix.bgu.ac.il
§gary@bgu.ac.il; URL: http://www.bgu.ac.il/~gary

The equation for the perturbations of the mean vorticity, $\widetilde{\mathbf{W}} = (\widetilde{W}_x(z), \widetilde{W}_y(z), 0)$, reads

$$\frac{\partial \widetilde{W}_x}{\partial t} = S\widetilde{W}_y + \nu_T \widetilde{W}_x'', \tag{2}$$

$$\frac{\partial \widetilde{W}_y}{\partial t} = -\beta_0 S l_0^2 \widetilde{W}_x'' + \nu_T \widetilde{W}_y'', \tag{3}$$

(see [11]), where $\widetilde{W}'' = \partial^2 \widetilde{W} / \partial z^2$, ν_T is the turbulent viscosity, l_0 is the maximum scale of turbulent motions and the parameter β_0 is of the order of 1, and depends on the scaling exponent of the correlation time of the turbulent velocity field (see Sec. II). A solution of Eqs. (2) and (3) has the form $\propto \exp(\gamma t + iK_z z)$, where the growth rate of the large-scale instability is given by $\gamma = \sqrt{\beta_0} S l_0 K_z - \nu_T K_z^2$ and K_z is the wave number. The maximum growth rate of perturbations of the mean vorticity, $\gamma_{\max} = \beta_0 (S l_0)^2 / 4\nu_T$, is attained at $K_z = K_m = \sqrt{\beta_0} S l_0 / 2\nu_T$. This corresponds to the ratio $\widetilde{W}_y / \widetilde{W}_x = \sqrt{\beta_0} l_0 K_m \approx S\tau_0$, where the time $\tau_0 = l_0 / u_0$ and u_0 is the characteristic turbulent velocity in the maximum scale l_0 of turbulent motions. Note that in a laminar flow this instability does not occur.

The mechanism of this instability is as follows (see [11] for details). The first term, $S\widetilde{W}_y = (\mathbf{W}^{(s)} \cdot \boldsymbol{\nabla})\widetilde{U}_x$, in Eq. (2) determines a "skew-induced" generation of perturbations of the mean vorticity $\widetilde{W}_x$ by stretching of the equilibrium mean vorticity $\mathbf{W}^{(s)} = (0, 0, S)$, where $\widetilde{\mathbf{U}}$ are the perturbations of the mean velocity. In particular, the mean vorticity $\widetilde{W}_x \mathbf{e}_x$ is generated from $\widetilde{W}_y \mathbf{e}_y$ by equilibrium shear motions with the mean vorticity $\mathbf{W}^{(s)}$, whereby $\widetilde{W}_x \mathbf{e}_x \propto (\mathbf{W}^{(s)} \cdot \boldsymbol{\nabla})\widetilde{U}_x \mathbf{e}_x \propto \widetilde{W}_y \mathbf{e}_y \times \mathbf{W}^{(s)}$. Here $\mathbf{e}_x$, $\mathbf{e}_y$, and $\mathbf{e}_z$ are the unit vectors along x, y, and

z axes, respectively. On the other hand, the first term, $-\beta_0 S l_0^2 \widetilde{W}_x''$, in Eq. (3) determines a "Reynolds stress-induced" generation of perturbations of the mean vorticity $\widetilde{W}_y$ by the Reynolds stresses. In particular, this term is determined by $(\nabla \times \mathbf{F})_y$. This implies that the component of the mean vorticity $\widetilde{W}_y \mathbf{e}_y$ is generated by an effective anisotropic viscous term $\propto -l_0^2 \Delta(\widetilde{W}_x \mathbf{e}_x \cdot \nabla) U^{(s)}(x) \mathbf{e}_y \propto -l_0^2 S \widetilde{W}_x'' \mathbf{e}_y$. This instability is caused by a combined effect of the sheared motions ("skew-induced" generation) and the "Reynolds stress-induced" generation of perturbations of the mean vorticity.

The mechanism for this large-scale instability in a sheared nonhelical homogeneous turbulence is different from that discussed in [12–14], where the generation of large-scale vorticity in the helical turbulence occurs due to hydrodynamic alpha effect. The latter effect is associated with the hydrodynamic helicity of turbulent flow. In a nonhelical homogeneous turbulence this effect does not occur.

The large-scale instability in a nonhelical homogeneous turbulence has been studied in [11] only for a simple case of unbounded turbulence with an imposed linear velocity shear and when the perturbations of the mean vorticity depend on one spatial variable z. In this study the theoretical approach proposed in [11] is further developed and applied for comprehensive investigation of the large-scale instability for different situations with nonuniform shear, inhomogeneous turbulence and a more general form of the perturbations of the mean vorticity $\widetilde{\mathbf{W}}(\mathbf{r})$ that depends on three spatial variables.

In the present study we consider three types of the background large-scale flows, i.e., the Couette flow (linear velocity shear) and Poiseuille flow (quadratic velocity shear) in a small-scale homogeneous turbulence, and the "log-linear" velocity shear in an inhomogeneous turbulence. We have derived mean-field equations for perturbations of large-scale velocity which depend on three spatial coordinates in a small-scale sheared turbulence, for a nonuniform background large-scale velocity shear and for an arbitrary scaling of the correlation time $\tau(k)$ of the turbulent velocity field.

The stability of the laminar Couette and Poiseuille flows in a problem of transition to turbulence has been studied in a number of publications (see, e.g., [15–20], and references therein). It is known that laminar plane Couette flow and antisymmetric mode of laminar plane Poiseuille flow are stable with respect to small perturbations for any Reynolds numbers. A symmetric mode of laminar plane Poiseuille flow is stable when the Reynolds number is less than 5772 [17]. In laminar flows the Tollmien-Schlichting waves can be excited. The molecular viscosity plays a destabilizing role in laminar flows which promotes the excitation of the Tollmien-Schlichting waves (see, e.g., [16]). These waves are growing solutions of the Orr-Sommerfeld equation.

In the present study we have found a turbulent analogue of the Tollmien-Schlichting waves. These waves are excited by a small-scale sheared turbulence, i.e., by a combined effect of the turbulent Reynolds stress-induced generation of perturbations of the mean vorticity and the background sheared motions. The energy of these waves is supplied by the small-scale sheared turbulence. We demonstrate that the off-diagonal terms in the turbulent viscosity tensor play a

crucial role in the excitation of the turbulent Tollmien-Schlichting waves. These waves can be excited even in a plane Couette flow imposed on a small-scale turbulence when perturbations of velocity depend on three spatial coordinates. When perturbations of large-scale velocity depend on one or two spatial coordinates the turbulent Tollmien-Schlichting waves can not be excited in a sheared turbulence. In the present study we show that the large-scale Couette and Poiseuille flows imposed on a small-scale turbulence can be unstable with respect to small perturbations. The critical effective Reynolds number (based on turbulent viscosity) required for the excitation of this large-scale instability, is of the order of 200.

This paper is organized as follows. In Sec. II the governing equations are formulated. In Sec. III we consider a homogeneous turbulence with a large-scale linear velocity shear (Couette flow), while in Sec. IV we study a homogeneous turbulence with a large-scale quadratic velocity shear (Poiseuille flow). In Sec. V we investigate formation of large-scale vortical structures in an inhomogeneous turbulence with an imposed nonuniform velocity shear. Finally, we draw conclusions in Sec. VI.

II. GOVERNING EQUATIONS

The equation for the mean velocity $\mathbf{U}$ in incompressible flow reads

$$\left(\frac{\partial}{\partial t} + \mathbf{U} \cdot \nabla\right) U_i = -\frac{\nabla_i P}{\rho} + \nabla_j \langle u_i u_j \rangle + \nu \Delta U_i, \qquad (4)$$

where $\mathbf{U}$ is the mean velocity, P is the mean pressure, and ν is the kinematic viscosity. The effect of turbulence on the mean flow is determined by the Reynolds stresses $\langle u_i u_j \rangle$, where $\mathbf{u}$ are the fluid velocity fluctuations.

We consider a turbulent flow with an imposed mean velocity shear $\nabla_i \mathbf{U}^{(s)}$. In order to study a stability of this equilibrium we consider perturbations $\widetilde{\mathbf{U}}$ of the mean velocity, i.e., the total mean velocity is $\mathbf{U} = \mathbf{U}^{(s)} + \widetilde{\mathbf{U}}$. Thus, the linearized equation for the small perturbations of the mean velocity is given by

$$\left(\frac{\partial}{\partial t} + \mathbf{U}^{(s)} \cdot \nabla\right) \widetilde{U}_i + (\widetilde{\mathbf{U}} \cdot \nabla) U_i^{(s)} = -\frac{\nabla_i \widetilde{P}}{\rho} + F_i + \nu \Delta \widetilde{U}_i,$$

$$(5)$$

where $F_i = -\nabla_j f_{ij}(\widetilde{\mathbf{U}})$ is the effective force, $f_{ij} = \langle u_i u_j \rangle$, and $\widetilde{P}$ are the perturbations of the fluid pressure. Equation (5) is derived by subtracting Eq. (4) written for the equilibrium velocity $\mathbf{U}^{(s)}$ from Eq. (4) for the mean velocity $\mathbf{U}$. We consider a simple large-scale velocity shear, so that $\mathbf{U}^{(s)}$ is directed along y direction and is nonuniform in x direction, i.e., $\mathbf{U}^{(s)} = (0, U_y^{(s)}(x), 0)$.

In order to obtain a closed system of equations, an equation for the effective force $F_i = -\nabla_j f_{ij}(\widetilde{\mathbf{U}})$ has been derived in [11], where

$$f_{ij}(\widetilde{\mathbf{U}}) = -2\nu_T(\partial\widetilde{U})_{ij} - l_0^2[4C_1M_{ij} + C_2(N_{ij} + H_{ij}) + C_3G_{ij}],$$
(6)

$(\partial\widetilde{U})_{ij} = (\nabla_i\widetilde{U}_j + \nabla_j\widetilde{U}_i)/2$ and l_0 is the maximum scale of turbulent motions. The tensors M_{ij}, N_{ij}, H_{ij}, and G_{ij}, in the expression for the Reynolds stresses (6) are given by

$$M_{ij} = (\partial U^{(s)})_{im}(\partial\widetilde{U})_{mj} + (\partial U^{(s)})_{jm}(\partial\widetilde{U})_{mi},$$

$$N_{ij} = \widetilde{W}_n[\varepsilon_{nim}(\partial U^{(s)})_{mj} + \varepsilon_{njm}(\partial U^{(s)})_{mi}],$$

$$H_{ij} = W_n^{(s)}[\varepsilon_{nim}(\partial\widetilde{U})_{mj} + \varepsilon_{njm}(\partial\widetilde{U})_{mi}],$$

$$G_{ij} = W_i^{(s)}\widetilde{W}_j + W_j^{(s)}\widetilde{W}_i,$$

ε_{ijk} is the fully antisymmetric Levi-Civita tensor, $(\partial U^{(s)})_{ij} = (\nabla_i U_j^{(s)} + \nabla_j U_i^{(s)})/2$ and the parameters C_k in Eq. (6) are given below.

The effective force F_i depends on the correlation time of the turbulent velocity field $\tau(k)$, where k is the wave number. In the present study we derive a more general form of the effective force F_i for an arbitrary scaling of the correlation time $\tau(k) = C\tau_0(k/k_0)^{-\mu}$ of the turbulent velocity field, where $k_0 = 1/l_0$. To this end we use Eq. (20) derived in [11]. The value of the coefficient $C = (q-1+\mu)/(q-1)$ corresponds to the standard form of the turbulent viscosity in the isotropic turbulence, i.e., $\nu_T = \int\tau(k)[\langle\mathbf{u}^2\rangle E(k)]dk = \tau_0\langle\mathbf{u}^2\rangle/3$. Here $E(k) = (q-1)k_0^{-1}(k/k_0)^{-q}$ is the energy spectrum of turbulence. For the Kolmogorov's type background turbulence (i.e., for the turbulence with a constant energy flux over the spectrum), the exponent $\mu = q-1$ and the coefficient $C = 2$. This case has been studied in [11]. For a turbulence with a scale-independent correlation time, the exponent $\mu = 0$ and the coefficient $C = 1$. The parameters C_k entering in the Reynolds stresses (6) are given by $C_1 = 2C^2(\mu^2 - 11\mu + 28)/315$, $C_2 = -C^2(7\mu+1)/90$ and $C_3 = -C^2(\mu+3)/90$.

For the derivation of the effective force F_i we use a procedure outlined below (see [11] for details). Using the equation for fluctuations of velocity written in a Fourier space, we derive equation for the two-point second-order correlation function of the velocity fluctuations $\langle u_i u_j\rangle$. We introduce a background turbulence with zero gradients of the mean fluid velocity. This background turbulence is determined by a stirring force that is independent of gradients of the mean velocity. In this study we use a model of isotropic, homogeneous and nonhelical background turbulence. Then we subtract the equation for the two-point second-order correlation function of the velocity fluctuations $\langle u_i u_j\rangle^{(0)}$ written for the background turbulence from the equation for $\langle u_i u_j\rangle$. This yields the equation for the deviations from the background turbulence.

The obtained second-moment equation include the first-order spatial differential operators $\hat{N}$ applied to the third-order moments $M^{(III)}$. A problem arises how to close the equation, i.e., how to express the third-order terms $\hat{N}M^{(III)}$ through the lower moments $M^{(II)}$ (see, e.g., [21–23]). To this end we use a spectral τ approximation which postulates that

the deviations of the third-moment terms from the contributions to these terms afforded by the background turbulence are expressed through the similar deviations of the second moments (see, e.g., [11,21,24–26]). A justification of the τ approximation for different situations has been performed in numerical simulations and analytical studies in [27–31].

We assume that the characteristic time of variation of the second moment of velocity fluctuations is substantially larger than the correlation time for all turbulence scales. This allows us to obtain a steady state solution of the second moment equation for the deviations from the background turbulence. Integration in $\mathbf{k}$ space allows us to determine the Reynolds stresses in the form of Eq. (6). Note that this form of the Reynolds stresses in a turbulent flow with a mean velocity shear can be obtained even by simple symmetry reasoning (see [11] for details).

In the following sections we use Eq. (5) with the derived effective force [see Eq. (6)] for a study of the dynamics of perturbations of the mean velocity. We show that under certain conditions the large-scale instability can be excited which causes formation of large-scale vortical structures.

III. LINEAR VELOCITY SHEAR (COUETTE FLOW) IN HOMOGENEOUS TURBULENCE

We consider a homogeneous turbulence with a mean linear velocity shear, $\mathbf{U}^{(s)} = (0, Sx, 0)$. This velocity field is a steady state solution of the Navier-Stokes equation. Let us first study the case when the velocity perturbations $\widetilde{\mathbf{U}}(t,x,z)$ are independent of y. The equations for the components $\widetilde{U}_x$ and $\widetilde{U}_y$ of the velocity perturbations read

$$\left[\frac{\partial}{\partial t} - \nu_T\Delta\right]\Delta\widetilde{U}_x = l_0^2 S\beta_0\Delta\nabla_z^2\widetilde{U}_y,$$
(7)

$$\Delta\left[\frac{\partial}{\partial t} - \nu_T\Delta\right]\widetilde{U}_y = -S\Delta\widetilde{U}_x,$$
(8)

and the component $\widetilde{U}_z$ is determined by the continuity equation $\nabla\cdot\widetilde{\mathbf{U}} = 0$, where $\beta_0 = C_1 + C_2 - C_3 = C^2(2\mu^2 - 43\mu + 63)/315$. In order to derive Eqs. (7) and (8) we calculate $\nabla\times(\nabla\times\widetilde{\mathbf{U}})$ using Eq. (5), that allows us to exclude the pressure term from this equation. We also use Eq. (6) for the Reynolds stresses in the sheared turbulence. For simplicity, in Eq. (8) we neglect the small terms $\sim O[(l_0/L_S)^2]$, where L_S is the characteristic scale of the velocity shear.

We seek for a solution of Eqs. (7) and (8) in the form

$$\widetilde{U}_{x,y} = \exp(\gamma t)[A_{x,y}\cos(K_x x) + B_{x,y}\cosh(K_z x)]\cos(K_z z + \phi),$$
(9)

where the coefficients $A_{x,y}$, $B_{x,y}$, the angle ϕ and the growth rate γ of the instability are determined by the boundary conditions. We choose the symmetric solution (relative the point $x=0$), because the maximum growth rate of the symmetric mode is higher than that of antisymmetric mode (see below). Perturbations of the mean velocity grow in time due to the large-scale instability with the growth rate

$$\gamma = \sqrt{\beta_0}\, Sl_0 K_z - \nu_T (K_x^2 + K_z^2). \tag{10}$$

The maximum growth rate of perturbations of the mean velocity,

$$\gamma_{\max} = \frac{\beta_0 (Sl_0)^2}{4\nu_T} - \nu_T K_x^2, \tag{11}$$

is attained at $K_z = K_m = \sqrt{\beta_0}\, Sl_0 / 2\nu_T$.

In order to determine the threshold required for the excitation of the large-scale instability, we consider the solution of Eqs. (7) and (8) with the following boundary conditions for a layer of the thickness L_S in the x direction: at $x = \pm L_S/2$ the functions $\widetilde{\mathbf{U}} = 0$ and $\nabla_x (\widetilde{U}_{x,y}) = 0$. This yields the threshold value of the wave number K_x^{cr}, determined by the equation

$$\tan(K_x^{\mathrm{cr}} L_S/2) = -\tanh(K_x^{\mathrm{cr}} L_S/2). \tag{12}$$

The condition $\gamma_{\max} > 0$ implies that $K_m \geq K_x^{\mathrm{cr}}$. Therefore, the large-scale instability is excited when the value of the shear S exceeds the critical value S_{cr} that is given by

$$S_{\mathrm{cr}} \tau_0 = \frac{2 K_x^{\mathrm{cr}} l_0}{3\sqrt{\beta_0}} \approx 4.7 \frac{l_0}{L_S}, \tag{13}$$

where $K_x^{\mathrm{cr}} = 2\pi / L_S$. Note that the value of K_x^{cr} for the symmetric mode is smaller than that for antisymmetric mode. This is the reason why the maximum growth rate of the symmetric mode is larger than that of antisymmetric mode.

Note that the parameter β_0 depends on the scaling exponent μ of the correlation time of the turbulent velocity field, $\tau(k) \propto k^{-\mu}$. In particular, for the Kolmogorov scaling, $\tau(k) \propto k^{-2/3}$, we arrive at $\beta_0 = 0.45$. This case has been considered in [11]. The necessary condition for the large-scale instability ($\beta_0 > 0$) reads $2\mu^2 - 43\mu + 63 > 0$, i.e., the instability is excited when $0 \leq \mu < 1.58$ and $\mu > 19.9$. Note that the condition $\mu > 19.9$ is not realistic. In the case of a turbulence with a scale-independent correlation time, the exponent $\mu = 0$ and the parameter $\beta_0 = 0.2$.

For small hydrodynamic Reynolds numbers, the scaling of the correlation time $\tau(k) \sim 1/(\nu k^2)$, i.e., $\mu = 2$, and the parameter $\beta_0 < 0$. This implies that the instability of the perturbations of the mean vorticity does not occur for small Reynolds numbers in agreement with the recent results obtained in [32] whereby an instability of the perturbations of the mean vorticity in a random flow with large-scale velocity shear has not been found using the second order correlation approximation and assumption that the correlation time $\tau(k) \sim 1/(\nu k^2)$. This approximation is valid only for small Reynolds numbers (see discussion in [33]).

Let us consider now a more general case when the velocity $\widetilde{\mathbf{U}}$ depends on three spatial coordinates, i.e., $\widetilde{\mathbf{U}} = \widetilde{\mathbf{U}}(t, x, y, z)$. The equations for the components $\widetilde{U}_x$ and $\widetilde{U}_y$ of the velocity perturbations read

$$\left(\frac{\partial}{\partial t} + U^{(s)} \nabla_y - \nu_T \Delta \right) \Delta \widetilde{U}_x = l_0^2 S \Delta [\beta_0 \Delta_H \widetilde{U}_y + (\beta_1$$
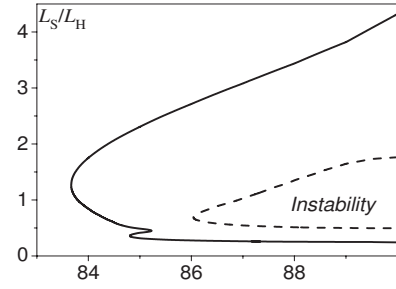$$- \beta_2) \nabla_x \nabla_y \widetilde{U}_x], \tag{14}$$

FIG. 1. Range of parameters (L_S/L_H; φ) for which the large-scale instability occurs for Couette background flow and for different values of the large-scale shear: $S\tau_0 = 0.2$ (dashed line); $S\tau_0 = 0.4$ (solid line). Here $L_S/l_0 = 30$.

$$\Delta \left(\frac{\partial}{\partial t} + U^{(s)} \nabla_y - \nu_T \Delta \right) \widetilde{U}_y = l_0^2 S \Delta [\beta_2 (\Delta - \nabla_y^2) \widetilde{U}_x + (\beta_1$$
$$- \beta_0) \nabla_x \nabla_y \widetilde{U}_y] + S(2\nabla_y^2 - \Delta) \widetilde{U}_x, \tag{15}$$

and the component $\widetilde{U}_z$ is determined by the continuity equation $\nabla \cdot \widetilde{\mathbf{U}} = 0$. Here $\Delta_H = \Delta - \nabla_x^2$, $\beta_1 = 2C_1 - C_2 = C^2(8\mu^2 - 39\mu + 231)/630$ and $\beta_2 = C_1 + C_3 = C^2(4\mu^2 - 51\mu + 91)/630$. In order to derive Eqs. (14) and (15) we calculate $\nabla \times (\nabla \times \widetilde{\mathbf{U}})$ using Eq. (5), that allows us to exclude the pressure term from this equation. For the derivation of Eqs. (14) and (15) we also use Eq. (6) for the Reynolds stresses in the sheared turbulence. Equations (14) and (15) can be reduced to the Orr-Sommerfeld equation if we replace ν_T by ν and set $\beta_n = 0$ (see, e.g., [15–17], and references therein).

We seek for a solution of Eqs. (14) and (15) in the form $\propto \Psi(x) \exp(\gamma t + i\omega t + i\mathbf{K}_H \cdot \mathbf{r})$, where $\mathbf{K}_H$ is the wave number that is perpendicular to the x axis. After the substitution of this solution into Eqs. (14) and (15) we obtain the system of the ordinary differential equations which is solved numerically. We consider the solution of Eqs. (14) and (15) with the following boundary conditions for a layer of the thickness L_S in the x direction: At $x = \pm L_S/2$ the functions $\widetilde{\mathbf{U}} = 0$ and $\nabla_x (\widetilde{U}_{x,y}) = 0$. These boundary conditions with a linear velocity shear corresponds to the Couette flow.

In this section we show that in a small-scale turbulence the large-scale Couette flow can be unstable under certain conditions. The range of parameters ($L_S/L_H; \varphi$) for which the large-scale instability occurs is shown in Fig. 1, where $L_H = 2\pi/K_H$, $K_H = (K_y^2 + K_z^2)^{1/2}$ and φ is the angle between the wave vector $\mathbf{K}_H$ and the direction of the mean sheared velocity $\mathbf{U}^{(s)}$. In Figs. 2–4 we show the growth rate of the large-scale instability $\gamma \tau_0$ and the frequencies of the generated modes $\omega \tau_0$ vs L_S/L_H. The growth rates of the large-scale instability increase with the increase of the angle φ, while the frequencies of the generated modes decrease with the angle φ so that $\omega(\varphi \to 90°) \to 0$. The growth rate of the large-scale instability reaches the maximum value at $\varphi = 90°$. In addition, the range of angles φ for which the large-scale instability occurs, is small and located in the vicinity of $\varphi = 90°$ (see Fig. 1). Therefore, $K_y \ll K_z$ and since $L_z \sim L_S$, the size of the
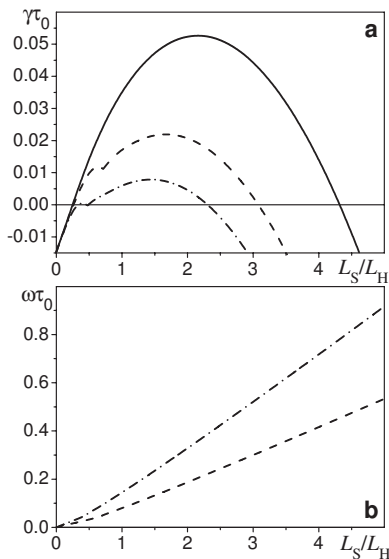
FIG. 2. Growth rate of (a) the large-scale instability $\gamma\tau_0$ and (b) frequencies $\omega\tau_0$ of the generated modes vs L_S/L_H for Couette background flow and for different angles φ: $\varphi=85°$ (dashed-dotted line), $\varphi=87°$ (dashed line), and $\varphi=90°$ (solid line). Here $S\tau_0=0.4$, $L_S/l_0=30$ and $\omega(\varphi=90°)=0$.

structures in the direction of $\mathbf{U}^{(s)}$ is much larger than the sizes of the structures along x and z directions. This implies that the large-scale structures formed due to this instability are stretched along the mean sheared velocity $\mathbf{U}^{(s)}$.

The curves in Figs. 2–4 have a point L_* whereby the first derivative of the growth rate of the large-scale instability with respect to the wave number K_H has a singularity. At this point there is a bifurcation which is illustrated in Fig. 3. In particular, the growth rates and the frequencies for the first and the second modes which have the highest growth rates
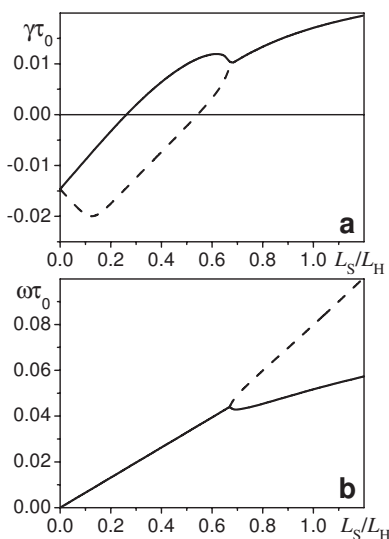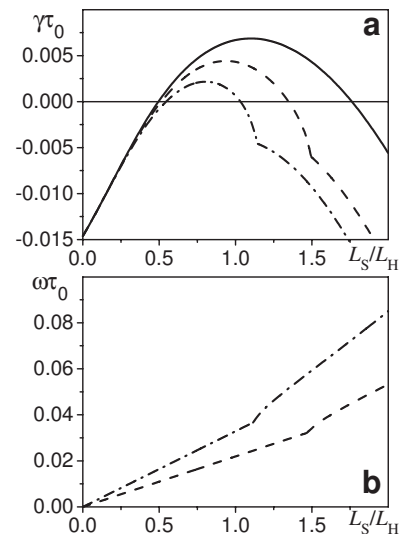

FIG. 3. (a) Growth rate $\gamma\tau_0$ and (b) the frequency $\omega\tau_0$ vs L_S/L_H of the first (solid line) and the second (dashed line) modes which have the highest growth rates for Couette background flow. Here the angle $\varphi=87°$, $S\tau_0=0.4$, and $L_S/l_0=30$.

FIG. 4. Growth rate of (a) the large-scale instability $\gamma\tau_0$ and (b) frequencies $\omega\tau_0$ of the generated modes vs L_S/L_H for Couette background flow and for different angles φ: $\varphi=87°$ (dashed-dotted line), $\varphi=88°$ (dashed line), and $\varphi=90°$ (solid line). Here $S\tau_0=0.2$, $L_S/l_0=30$, and $\omega(\varphi=90°)=0$.

are shown in Fig. 3(a) and 3(b). When the size of perturbations $L_H<L_*$, the frequencies of the first and the second modes are different, but the growth rates are the same. Therefore, at the point $L_H=L_*$, there is a generation of two different modes with the same growth rate. On the other hand, when the size of perturbations $L_H>L_*$, the growth rates of the first and the second modes are different, but the frequencies are the same.

The maximum growth rate of perturbations of the mean velocity, $\gamma_{\max}$, is attained at $K_H=K_m$, and the value K_m increases with the increase of the angle φ between the wave vector $\mathbf{K}_H$ and the direction of the mean sheared velocity $\mathbf{U}^{(s)}$. The increase of shear S promotes the large-scale instability, i.e., it cause the increase of the range for the instability (see Fig. 1) and the maximum growth rate (see Figs. 2 and 4). The characteristic spatial scale $L_m=2\pi/K_m$ and the time scale $t_{\mathrm{inst}}\sim\gamma_{\max}^{-1}$ for the instability are much larger than the characteristic turbulent scales. This justifies separation of scales which is required for the validity of the mean-field theory applied in the present study. The spatial profiles of the ratios of vorticity components $\widetilde{W}_y/\widetilde{W}_x$ and $\widetilde{W}_z/\widetilde{W}_x$ for perturbations in Couette background flow are shown in Fig. 5. The function $\widetilde{W}_y/\widetilde{W}_x$ is symmetric relative to the center of the flow at $x=0$, while the function $\widetilde{W}_z/\widetilde{W}_x$ is antisymmetric. Since the function $\widetilde{W}_x\to0$ at the boundaries of the flow, the ratios of vorticity components $\widetilde{W}_y/\widetilde{W}_x$ and $\widetilde{W}_z/\widetilde{W}_x$ tend to $\to\pm\infty$ at the boundaries.

The numerical results for the case $\varphi=90°$ shown in Figs. 2, 4, and 5 coincide with the analytical predictions based on Eqs. (9)–(13). For instance, the threshold value of the shear at $L_S/l_0=30$ is $S_{\mathrm{cr}}\tau_0\approx0.157$ in agreement with Eq. (13). The ratio of vorticity components $\widetilde{W}_y/\widetilde{W}_x\approx0.3$ at $x=0$ for modes with the maximum growth rate of the large-scale instability. This is in agreement with this ratio of $\widetilde{W}_y/\widetilde{W}_x$ obtained using
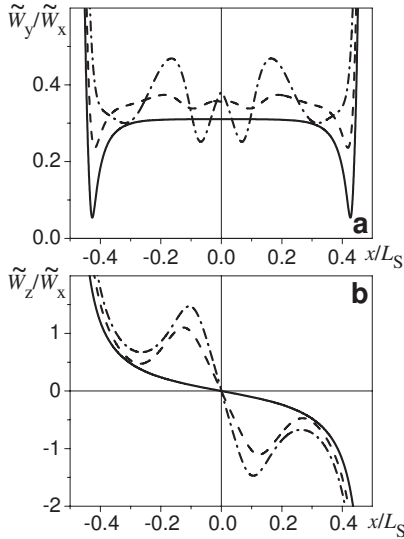
FIG. 5. Spatial profiles of the ratios of vorticity components (a) $\widetilde{W}_y/\widetilde{W}_x$ and (b) $\widetilde{W}_z/\widetilde{W}_x$ for modes with the maximum growth rates of the large-scale instability in Couette background flow and for different angles φ: $\varphi=85°$ (dashed-dotted line), $\varphi=87°$ (dashed line), and $\varphi=90°$ (solid line). Here $S\tau_0=0.4$ and $L_S/l_0=30$.

Eq. (9). The maximum growth rates of perturbations of the mean velocity are in agreement with Eqs. (11) and (12). When we switch off the turbulence, the large-scale instability does not excited, etc.

The growing modes with a nonzero frequency discussed in this section can be regarded as the turbulent analogue of the Tollmien-Schlichting waves. In laminar flows the Tollmien-Schlichting waves are growing solutions of the Orr-Sommerfeld equation and the molecular viscosity promotes the excitation of the Tollmien-Schlichting waves (see, e.g., [16]). On the other hand, the turbulent Tollmien-Schlichting waves are excited by a small-scale sheared turbulence, i.e., by a combined effect of the turbulent Reynolds stress-induced generation of perturbations of the mean vorticity and the background sheared motions.

IV. QUADRATIC VELOCITY SHEAR (POISEUILLE FLOW) IN HOMOGENEOUS TURBULENCE

Now we consider a homogeneous turbulence with an imposed large-scale quadratic velocity shear, $\mathbf{U}^{(s)}=S_*x(1-x/L_S)\mathbf{e}_y$. The equations for the components $\widetilde{U}_x$ and $\widetilde{U}_y$ of the velocity perturbations read

$$\left(\frac{\partial}{\partial t}+U^{(s)}\nabla_y-\nu_T\Delta\right)\Delta\widetilde{U}_x=l_0^2 S\Delta[\beta_0\Delta_H\widetilde{U}_y+(\beta_1$$
$$-\beta_2)\nabla_x\nabla_y\widetilde{U}_x]+S'\nabla_y\widetilde{U}_y, \tag{16}$$

$$\Delta\left(\frac{\partial}{\partial t}+U^{(s)}\nabla_y-\nu_T\Delta\right)\widetilde{U}_y=S(2\nabla_y^2-\Delta)\widetilde{U}_x-2S'\nabla_x\widetilde{U}_x$$
$$+l_0^2 S\Delta[(\beta_1-\beta_0)\nabla_x\nabla_y\widetilde{U}_y+\beta_2(\Delta$$
$$-\nabla_y^2)\widetilde{U}_x]+l_0^2 S'[2\beta_1\nabla_x\nabla_y(\nabla_x\widetilde{U}_y$$
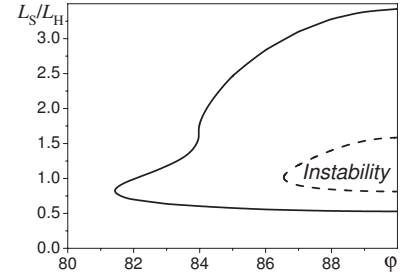

FIG. 6. Range of parameters (L_S/L_H; φ) for which the large-scale instability for Poiseuille background flow occurs, and for different values of the large-scale shear: $S_*\tau_0=0.5$ (dashed line) and $S_*\tau_0=0.6$ (solid line). Here $L_S/l_0=30$ and $S_*=S(x=0)$.

$$-\nabla_y\widetilde{U}_x)+\Delta[(2\beta_2+\beta_1)\nabla_x\widetilde{U}_x$$
$$+(\beta_2-\beta_0)\nabla_y\widetilde{U}_y]], \tag{17}$$

and the component $\widetilde{U}_z$ is determined by the continuity equation $\boldsymbol{\nabla}\cdot\widetilde{\mathbf{U}}=0$, where $S(x)=\nabla_x U^{(s)}$ and $S'=\nabla_x S$. In order to derive Eqs. (16) and (17) we calculate $\boldsymbol{\nabla}\times(\boldsymbol{\nabla}\times\widetilde{\mathbf{U}})$ using Eq. (5). We seek for a solution of Eqs. (16) and (17) in the form $\propto\Psi(x)\exp(\gamma t+i\omega t+i\mathbf{K}_H\cdot\mathbf{r})$, where $\mathbf{K}_H$ is the wave number that is perpendicular to the x axis. After the substitution of this solution into Eqs. (16) and (17) we obtain the system of the ordinary differential equations which is solved numerically. We consider the solution of Eqs. (16) and (17) with the following boundary conditions for a layer of the thickness L_S in the x direction: At $x=\pm L_S/2$ the functions $\widetilde{\mathbf{U}}=0$ and $\nabla_x(\widetilde{U}_{x,y})=0$. These boundary conditions with a quadratic large-scale velocity shear corresponds to the Poiseuille flow. We show below that in a small-scale turbulence the large-scale Poiseuille flow can be unstable with respect to small perturbations.

The range of parameters (L_S/L_H; φ) for which the large-scale instability in the Poiseuille background flow occurs is shown in Fig. 6 for different values of the large-scale shear, where $S_*=S(x=0)$. The growth rates of this instability and the frequencies of the generated turbulent Tollmien-Schlichting waves are shown in Figs. 7 and 8. The spatial profiles of the ratios of vorticity components $\widetilde{W}_y/\widetilde{W}_x$ and $\widetilde{W}_z/\widetilde{W}_x$ in Poiseuille background flow for modes with the maximum growth rates of the large-scale instability are shown in Fig. 9. The general behavior of the large-scale instability in the Poiseuille background flow is similar to that for the Couette background flow. In particular, the growth rates of the large-scale instability increase with the increase of the angle φ between the wave vector $\mathbf{K}_H$ and the direction of the mean sheared velocity $\mathbf{U}^{(s)}$, reaching the maximum value at $\varphi=90°$. The frequencies $\omega\tau_0$ of the generated turbulent Tollmien-Schlichting waves by the large-scale instability decrease with the increase of the angle φ and $\omega\to0$ at $\varphi\to90°$. The values K_m at which the growth rates of the large-scale instability reach the maximum values increase with the increase of the angle φ. The range for the large-scale instability and the growth rates of perturbations in the Poiseuille
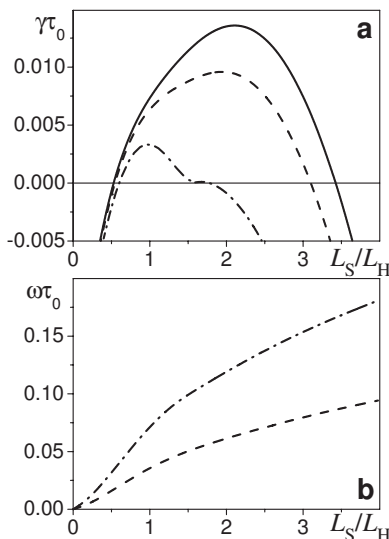
FIG. 7. Growth rate of (a) the large-scale instability $\gamma\tau_0$ and (b) frequencies $\omega\tau_0$ of the generated modes vs L_S/L_H for Poiseuille background flow and for different angles φ: $\varphi=84°$ (dashed-dotted line), $\varphi=87°$ (dashed line), $\varphi=90°$ (solid line). Here $S_*\tau_0=0.6$, $L_S/l_0=30$ and $\omega(\varphi=90°)=0$.

background flow increases with the increase of shear. This implies that increase of shear promotes the large-scale instability.

For the Poiseuille flow the large-scale instability can be excited for smaller angles φ than that for the Couette background flow. On the other hand, the thresholds for the instability in the value of shear and in the value of L_S/L_H for Poiseuille background flow are larger than that for the Couette background flow. A difference between the Couette and Poiseuille background flows can be also seen in Figs. 5 and 9
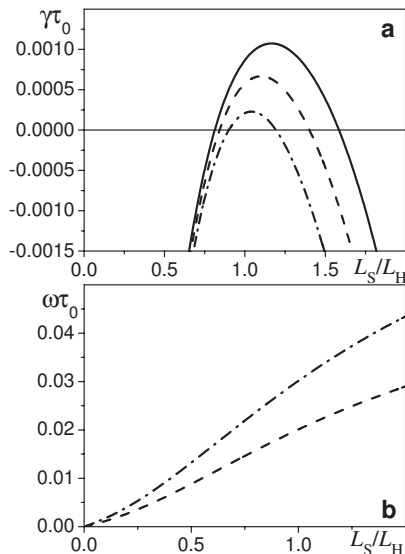

FIG. 8. Growth rate of (a) the large-scale instability $\gamma\tau_0$ and (b) frequencies $\omega\tau_0$ of the generated modes vs L_S/L_H for Poiseuille background flow and for different angles φ: $\varphi=87°$ (dashed-dotted line), $\varphi=88°$ (dashed line), and $\varphi=90°$ (solid line). Here $S_*\tau_0=0.5$, $L_S/l_0=30$, and $\omega(\varphi=90°)=0$.

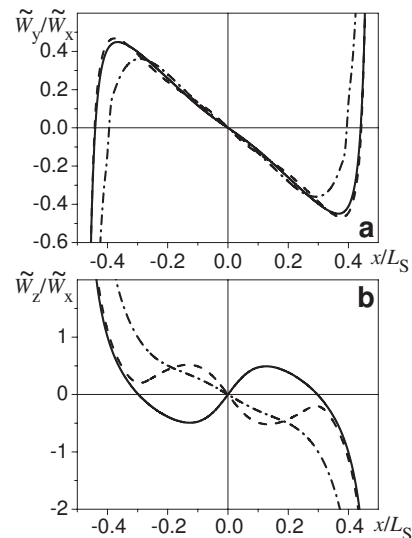FIG. 9. Spatial profiles of the ratios of vorticity components (a) $\widetilde{W}_y/\widetilde{W}_x$ and (b) $\widetilde{W}_z/\widetilde{W}_x$ for modes with the maximum growth rates of the large-scale instability in Poiseuille background flow and for different angles φ: $\varphi=84°$ (dashed-dotted line), $\varphi=87°$ (dashed line), and $\varphi=90°$ (solid line). Here $S_*\tau_0=0.6$ and $L_S/l_0=30$.

for the spatial profiles of the ratios of vorticity components $\widetilde{W}_y/\widetilde{W}_x$ and $\widetilde{W}_z/\widetilde{W}_x$. This difference is caused by the different geometries in these flows. In particular, the first spatial derivatives of the flow velocity in the Poiseuille background flow are antisymmetric relative to the center of the flow at $x=0$, while they are symmetric (constant) in the Couette background flow. This is the reason of that the spatial profile of $\widetilde{W}_y/\widetilde{W}_x$ is symmetric relative to $x=0$ in the Couette background flow, and it is antisymmetric in the Poiseuille flow.

V. NONUNIFORM VELOCITY SHEAR IN INHOMOGENEOUS TURBULENCE

In this section we consider a more complicated form of nonuniform velocity shear in an inhomogeneous turbulence. For simplicity we consider the case when the small perturbations of the mean velocity $\widetilde{\mathbf{U}}$ are independent of y. The equations for the components $\widetilde{U}_x$ and $\widetilde{U}_y$ of the velocity perturbations in an inhomogeneous turbulence with a nonuniform shear read

$$\Delta\left[\frac{\partial}{\partial t}-\nu_T\Delta\right]\widetilde{U}_x=\beta_0[l_0^2 S\Delta-\nabla_x^2(l_0^2 S)]\nabla_z^2\widetilde{U}_y-2(\nabla_x^2\nu_T)\nabla_z^2\widetilde{U}_x,$$

$$(18)$$

$$\left[\frac{\partial}{\partial t}-\nu_T\Delta\right]\widetilde{U}_y=[-S+\beta_1\nabla_x(l_0^2 S)\nabla_x+\beta_2 l_0^2 S\Delta]\widetilde{U}_x$$

$$+(\nabla_x\nu_T)\nabla_x\widetilde{U}_y, \qquad (19)$$

and the component $\widetilde{U}_z$ is determined by the continuity equation $\boldsymbol{\nabla}\cdot\widetilde{\mathbf{U}}=0$, where $S(x)=\nabla_x U^{(s)}$. Equation (19) is the y component of Eq. (5) with $\nabla_y\widetilde{P}=0$, while Eq. (18) is the x
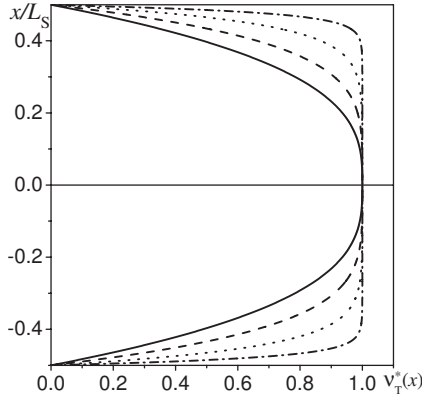
FIG. 10. Spatial profile of the normalized turbulent viscosity $\nu_T^*(x)$ for different values of the parameter α: $\alpha=6$ (solid line), $\alpha=10$ (dashed line), $\alpha=20$ (dotted line), and $\alpha=50$ (dashed-dotted line).

component of $\boldsymbol{\nabla} \times (\boldsymbol{\nabla} \times \widetilde{\mathbf{U}})$ determined from Eq. (5). We consider the solution of Eqs. (18) and (19) with the following boundary conditions for a layer of the thickness L_S in the x direction: at $x=\pm L_S/2$ the functions $\widetilde{\mathbf{U}}=0$ and $\boldsymbol{\nabla}_x(\widetilde{U}_{x,y})=0$.

We consider a "log-linear" velocity profile for the background large-scale flow in an inhomogeneous turbulence. In particular, we use the following relationship for the velocity shear $S(x)=u_\star^2/\nu_T(x)$ and the eddy viscosity $\nu_T(x)=u_\star l_0(x)$, where $l_0(x)=\kappa\eta(x)L_S$ is the turbulence length scale, κ is the von Kármán constant, $u_\star$ is the friction velocity, $\eta(x)$ is the dimensionless function that characterizes the spatial profile of the background velocity shear and inhomogeneity of small-scale turbulence (see below). These relationships are usually used for the logarithmic boundary layer profiles (see, e.g., [22]). The spatial profile $\eta(x)$ for $0 \leq x \leq L_S/2$ is chosen in the form

$$\eta(x) = a_1[1 - \exp(-a_0\tilde{x})] + a_2\tilde{x} + a_3\tilde{x}^2 + a_4\tilde{x}^3, \quad (20)$$

where $\tilde{x}=x/L_S-1/2$, the coefficients a_k are determined by the following conditions: At $x=0$ the functions $\eta=1$, $\nabla_x\eta=0$, $\nabla_x^2\eta=0$, $\nabla_x^3\eta=0$, and at $x=-L_S/2$ the derivative $\nabla_x\eta=\alpha/L_S$. Here α is a free parameter that characterizes the inhomogeneities of small-scale turbulence. The spatial profile of the normalized turbulent viscosity $\nu_T^*(x)=\nu_T(x)/(\kappa u_\star L_S) \equiv \eta(x)$ is shown in Fig. 10 for different values of the parameter α. The function $\nu_T^*(x)$ is chosen to be symmetric relative the point $x=0$. The minimum possible value of the parameter α is $\alpha=6$. We have chosen the velocity shear profile $U^{(s)}(x)$ so that the logarithmic velocity profile near the boundaries can be matched with the linear shear velocity for the central part of the background flow. Such kind of flow is typical for the atmospheric boundary layer. Figure 11 shows the mean velocity profile $U^{(s)}(x)/U_{max}$ for different values of the parameter α, where $U_{max}=u_\star/\kappa$.

We seek for a solution of Eqs. (18) and (19) in the form $\propto \Psi(x)\exp(\gamma t+iK_z z)$. After the substitution of this solution into Eqs. (18) and (19) we obtain the system of the ordinary differential equations which is solved numerically. The growth rate $\gamma\tau_0$ of the large-scale instability versus l_{max}/L_z is
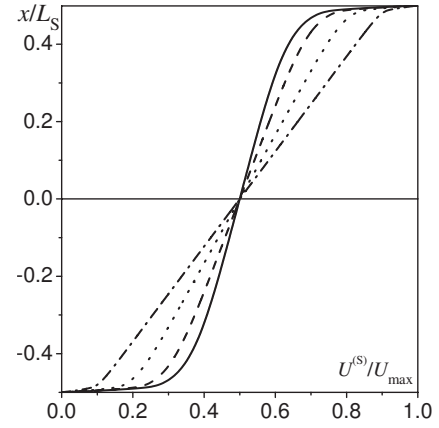

FIG. 11. Mean velocity profile $U^{(s)}(x)/U_{max}$ for different values of the parameter α: $\alpha=6$ (solid line), $\alpha=10$ (dashed line), $\alpha=20$ (dotted line), and $\alpha=50$ (dashed-dotted line), where $U_{max}=u_\star/\kappa$.

shown in Fig. 12, where $L_z=2\pi/K_z$ is the size of perturbations in z direction and $l_{max}=\kappa L_S$ is the maximum value of the turbulent length scale l_0 when $\eta \to 1$ ($x \to 1$). The range of parameters (l_{max}/L_z; α) for which the large-scale instability occurs is shown in Fig. 13(a). The vertical dashed line in Fig. 13 indicates that the minimum possible value of the parameter α is $\alpha_{min}=6$. Figure 13(b) demonstrates that the increase of the parameter α causes the increase of the maximum growth rate of the large-scale instability. The growth rate of the large-scale instability for the inhomogeneous turbulence with a large-scale nonuniform shear is much larger than that for the Couette and Poiseuille background flows.

The spatial profiles of the ratios of vorticity components $\widetilde{W}_y/\widetilde{W}_x$ and $\widetilde{W}_z/\widetilde{W}_x$ for modes with the maximum growth rates of the large-scale instability are shown in Fig. 14. These profiles are different from that for the Couette and Poiseuille background flows. The components $\widetilde{W}_y$ and $\widetilde{W}_z$ of perturbations of the mean vorticity in the central part of the flow are usually much smaller than the component $\widetilde{W}_x$. Inspection of Figs. 12 and 13(a) shows that the parameter $l_{max}/L_z < 0.17$. The characteristic time scale for the instability is much larger
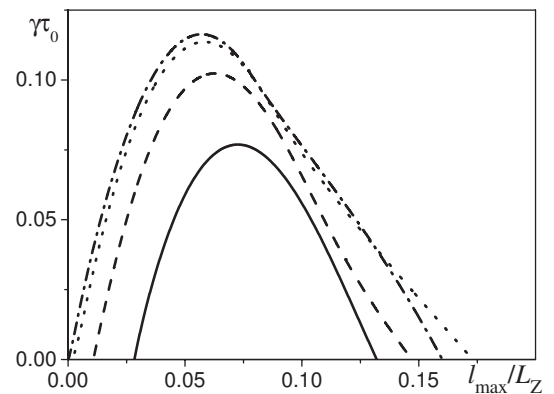

FIG. 12. Growth rate of the large-scale instability versus l_{max}/L_z in inhomogeneous turbulence with nonuniform velocity shear for different values of the parameter α: $\alpha=6$ (solid line), $\alpha=10$ (dashed line), $\alpha=20$ (dotted line), and $\alpha=50$ (dashed-dotted line). Here $l_{max}=l_0(x \to 0.5L_z)$.
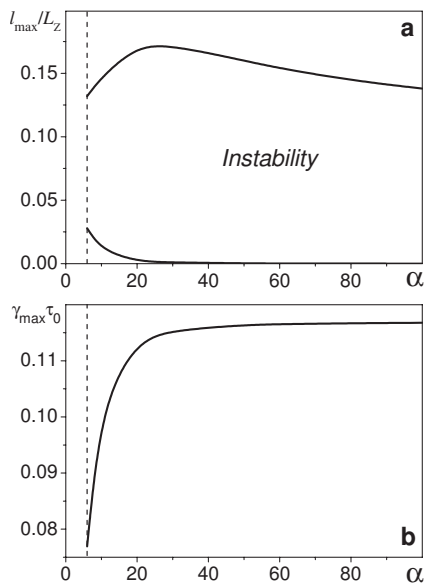
FIG. 13. (a) Range of parameters (l_{max}/L_z; α) for which the large-scale instability in inhomogeneous turbulence with nonuniform velocity shear occurs. (b) Maximum growth rate $\gamma_{max}\tau_0$ of the large-scale instability versus the parameter α. Here $l_{max}=l_0(x \rightarrow 0.5L_z)$.

than the characteristic turbulent time. This justifies separation of scales which is required for the validity of the mean-field theory used here.

Note that in the interval $-L_S/2 \leq x \leq 0$ the obtained results discussed in this section imply a stability theory for the turbulent boundary layer. Our study shows that the turbulent boundary layer can be unstable under certain conditions.
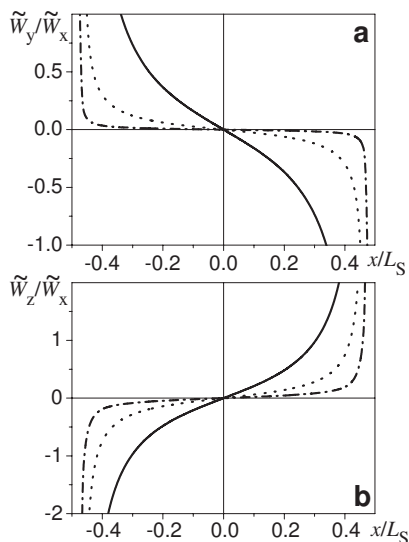

FIG. 14. Spatial profiles of the ratios of vorticity components (a) $\tilde{W}_y/\tilde{W}_x$ and (b) $\tilde{W}_z/\tilde{W}_x$ for modes with the maximum growth rates of the large-scale instability in inhomogeneous turbulence with nonuniform velocity shear for different values of the parameter α: $\alpha=6$ (solid line), $\alpha=20$ (dashed line), and $\alpha=50$ (dashed-dotted line). Here $l_{max}=l_0(x \rightarrow 0.5L_z)$.

VI. DISCUSSION

In this study the theoretical approach proposed in [11] is further developed and applied to investigate the large-scale instability in a nonhelical turbulence with a nonuniform shear and a more general form of the perturbations of the mean vorticity. In particular, we consider three types of the background large-scale sheared flows imposed on small-scale turbulence: Couette flow (linear velocity shear) and Poiseuille flow (quadratic velocity shear) in a small-scale homogeneous turbulence, and a more complicated nonuniform velocity shear with the logarithmic velocity profile near the boundaries matched with the linear shear velocity for the central part of the background flow. This nonuniform velocity shear is imposed on an inhomogeneous turbulence. The latter flow is typical for the atmospheric boundary layer.

We show that the large-scale Couette and Poiseuille flows imposed on a small-scale turbulence are unstable with respect to small perturbations due to the excitation of the large-scale instability. This instability causes generation of large-scale vorticity and formation of large-scale vortical structures. The size of the formed vortical structures in the direction of the background velocity shear is much larger than the sizes of the structures in the directions perpendicular to the velocity shear. Therefore, the large-scale structures formed during this instability are stretched along the mean sheared velocity. Increase of shear promotes the large-scale instability. The thresholds for the excitation of the large-scale instability in the value of shear and the aspect ratio of structures for Poiseuille background flow are larger than that for the Couette background flow. The growth rate of the large-scale instability for the inhomogeneous turbulence with the "log-linear" velocity shear is much larger than that for the Couette and Poiseuille background flows. The characteristic spatial and time scales for the instability are much larger than the characteristic turbulent scales. This justifies separation of scales which is required for the validity of the mean-field theory applied in the present study.

The large-scale instability results in excitation of the turbulent Tollmien-Schlichting waves. The mechanism for the excitation of these waves is different from that for the Tollmien-Schlichting waves in laminar flows. In particular, the molecular viscosity plays a crucial role in the excitation of the Tollmien-Schlichting waves in laminar flows. Contrary, the turbulent Tollmien-Schlichting waves are excited by a combined effect of the turbulent Reynolds stress-induced generation of perturbations of the mean vorticity and the background sheared motions. The energy of these waves is supplied by the small-scale sheared turbulence, and the off-diagonal terms in the turbulent viscosity tensor play a crucial role in the excitation of the turbulent Tollmien-Schlichting waves.

Note that this study is principally different from the problems of transition to turbulence whereby the stability of the laminar Couette and Poiseuille flows are investigated (see, e.g., [15–20], and references therein). Here we do not analyze a transition to turbulence. We study the large-scale instability caused by an effect of the small-scale anisotropic turbulence on the mean flow. This anisotropic turbulence is produced by an interaction of equilibrium large-scale Cou-

ette or Poiseuille flows with a small-scale isotropic background turbulence produced by, e.g., a stirring force. The anisotropic velocity fluctuations are generated by tangling of the mean-velocity gradients with the velocity fluctuations of the background turbulence [11,26].

The "tangling" mechanism is an universal phenomenon that was introduced in [34,35] for a passive scalar and in [36,37] for a passive vector (magnetic field). The Reynolds stresses in a turbulent flow with a mean velocity shear is another example of tangling anisotropic fluctuations [38]. For instance, these velocity fluctuations are anisotropic in the presence of shear and have a steeper spectrum $\propto k^{-7/3}$ than, e.g., a Kolmogorov background turbulence (see, e.g., [26,38–41]). The anisotropic velocity fluctuations determine the effective force and the Reynolds stresses in Eq. (6). This is the reason for the new terms $\propto \beta_n l_0^2$ appearing in Eqs. (14)–(19).

The obtained results in this study may be of relevance in different turbulent astrophysical, geophysical, and industrial flows. Turbulence with a large-scale velocity shear is a universal feature in astrophysics and geophysics. In particular, the analyzed effects may be important, e.g., in accretion disks, extragalactic clusters, merged protostellar and protogalactic clouds. Sheared motions between interacting clouds can cause an excitation of the large-scale instability which results in generation of the mean vorticity and formation of large-scale vortical structures (see, e.g., [42–44]). Dust particles can be trapped by the vortical structures to enhance agglomeration of material and formation of particle clusters [45–49].

The suggested mechanism can be used in the analysis of the flows associated with Prandtl's turbulent secondary flows (see, e.g., [7,10]). However, in this study we have investigated only simple physical mechanisms to describe an initial (linear) stage of the formation of vortical structures. The simple models considered in this study can only mimic the flows associated with turbulent secondary flows. Clearly, the comprehensive numerical simulations of the nonlinear problem are required for quantitative description of the turbulent secondary flows.

ACKNOWLEDGMENTS

[1] H. J. Lugt, *Vortex Flow in Nature and Technology* (J. Wiley and Sons, New York, 1983), and references therein.

[2] J. Pedlosky, *Geophysical Fluid Dynamics* (Springer, New York, 1987), and references therein.

[3] A. J. Chorin, *Vorticity and Turbulence* (Springer, New York, 1994), and references therein.

[4] A. Glasner, E. Livne, and B. Meerson, Phys. Rev. Lett. **78**, 2112 (1997).

[5] A. Tsinober, Eur. J. Mech. B/Fluids **17**, 421 (1998).

[6] C. Reyl, T. M. Antonsen, and E. Ott, Physica D **111**, 202 (1998).

[7] L. Prandtl, *Essentials of Fluid Dynamics* (Blackie, London, 1952).

[8] A. A. Townsend, *The Structure of Turbulent Shear Flow* (Cambridge University Press, Cambridge, UK, 1956).

[9] H. J. Perkins, J. Fluid Mech. **44**, 721 (1970).

[10] P. Bradshaw, Annu. Rev. Fluid Mech. **19**, 53 (1987).

[11] T. Elperin, N. Kleeorin, and I. Rogachevskii, Phys. Rev. E **68**, 016311 (2003).

[12] S. S. Moiseev, R. Z. Sagdeev, A. V. Tur, G. A. Khomenko, and A. M. Shukurov, Sov. Phys. Dokl. **28**, 925 (1983) [Dokl. Acad. Nauk SSSR **273**, 549 (1983)].

[13] G. A. Khomenko, S. S. Moiseev, and A. V. Tur, J. Fluid Mech. **225**, 355 (1991).

[14] O. G. Chkhetiany, S. S. Moiseev, A. S. Petrosyan, and R. Z. Sagdeev, Phys. Scr. **49**, 214 (1994).

[15] P. G. Drazin and W. H. Reid, *Hydrodynamic Stability* (Cambridge University Press, Cambridge, UK, 1981).

[16] P. J. Schmid and D. S. Henningson, *Stability and Transition in Shear Flows* (Springer, Berlin, 2001).

[17] W. O. Criminale, T. L. Jackson, and R. D. Joslin, *Theory and Computation of Hydrodynamic Stability* (Cambridge University Press, Cambridge, UK, 2003).

[18] B. J. Bayly, S. A. Orszag, and Th. Herbert, Annu. Rev. Fluid Mech. **20**, 359 (1988).

[19] D. Rempfer, Annu. Rev. Fluid Mech. **35**, 229 (2003).

[20] B. Eckhardt, T. M. Schneider, B. Hof, and J. Westerweel, Annu. Rev. Fluid Mech. **39**, 447 (2007).

[21] S. A. Orszag, J. Fluid Mech. **41**, 363 (1970).

[22] A. S. Monin and A. M. Yaglom, *Statistical Fluid Mechanics* (MIT Press, Cambridge, MA, 1975).

[23] W. D. McComb, *The Physics of Fluid Turbulence* (Clarendon, Oxford, 1990).

[24] A. Pouquet, U. Frisch, and J. Leorat, J. Fluid Mech. **77**, 321 (1976).

[25] N. Kleeorin, I. Rogachevskii, and A. Ruzmaikin, Zh. Eksp. Teor. Fiz. **97**, 1555 (1990) [Sov. Phys. JETP **70**, 878 (1990)].

[26] T. Elperin, N. Kleeorin, I. Rogachevskii, and S. S. Zilitinkevich, Phys. Rev. E **66**, 066305 (2002).

[27] E. G. Blackman and G. B. Field, Phys. Rev. Lett. **89**, 265007 (2002); Phys. Fluids **15**, L73 (2003).

[28] G. Field and E. G. Blackman, Astrophys. J. **572**, 685 (2002).

[29] A. Brandenburg, P. Käpylä, and A. Mohammed, Phys. Fluids **16**, 1020 (2004).

[30] A. Brandenburg and K. Subramanian, Phys. Rep. **417**, 1 (2005); Astron. Astrophys. **439**, 835 (2005).

[31] S. Sur, K. Subramanian, and A. Brandenburg, Mon. Not. R. Astron. Soc. **376**, 1238 (2007).

[32] G. Rüdiger and L. L. Kitchatinov, Astron. Nachr. **327**, 298 (2006).

[33] I. Rogachevskii, N. Kleeorin, and E. Liverts, Geophys. Astrophys. Fluid Dyn. **100**, 537 (2006); I. Rogachevskii and N.

Kleeorin, Phys. Rev. E **75**, 046305 (2007).

[34] A. D. Wheelon, Phys. Rev. **105**, 1706 (1957).

[35] G. K. Batchelor, I. D. Howells, and A. A. Townsend, J. Fluid Mech. **5**, 134 (1959).

[36] G. S. Golitsyn, Dokl. Acad. Nauk **132**, 315 (1960) [Sov. Phys. Dokl. **5**, 536 (1960)].

[37] H. K. Moffatt, J. Fluid Mech. **11**, 625 (1961).

[38] J. L. Lumley, Phys. Fluids **10**, 1405 (1967).

[39] J. C. Wyngaard and O. R. Cote, Q. J. R. Meteorol. Soc. **98**, 590 (1972).

[40] S. G. Saddoughi and S. V. Veeravalli, J. Fluid Mech. **268**, 333 (1994).

[41] T. Ishihara, K. Yoshida, and Y. Kaneda, Phys. Rev. Lett. **88**, 154501 (2002).

[42] P. J. E. Peebles, *The Large Scale Structure of the Universe* (Princeton University Press, Princeton, NJ, 1980).

[43] Ya. B. Zeldovich and I. D. Novikov, *Relativistic Astrophysics, Vol. 2, The Structure and Evolution of the Universe* (Chicago University Press, Chicago, 1983).

[44] A. D. Chernin, Astron. Astrophys. **267**, 315 (1993); Astrophys. Space Sci. **186**, 159 (1991).

[45] P. Barge and J. Sommeria, Astron. Astrophys. **295**, L1 (1995).

[46] L. S. Hodgson and A. Brandenburg, Astron. Astrophys. **330**, 1169 (1998).

[47] T. Elperin, N. Kleeorin and I. Rogachevskii, Phys. Rev. Lett. **81**, 2898 (1998).

[48] P. H. Chavanis, Astron. Astrophys. **356**, 1089 (2000).

[49] A. Johansen, A. C. Andersen, and A. Brandenburg, Astron. Astrophys. **417**, 361 (2004).